Exchange-coupling in thermal annealed bimagnetic core/shell nanoparticles

G.C. Lavorato, E. Lima Jr., H.E. Troiani, R.D. Zysler, E.L. Winkler

PII: S0925-8388(15)00476-4
DOI: http://dx.doi.org/10.1016/j.jallcom.2015.02.050
Reference: JALCOM 33424

To appear in: *Journal of Alloys and Compounds*

Received Date: 12 January 2015
Revised Date: 5 February 2015
Accepted Date: 6 February 2015

Please cite this article as: G.C. Lavorato, E. Lima Jr., H.E. Troiani, R.D. Zysler, E.L. Winkler, Exchange-coupling in thermal annealed bimagnetic core/shell nanoparticles, *Journal of Alloys and Compounds* (2015), doi: http://dx.doi.org/10.1016/j.jallcom.2015.02.050

Exchange-coupling in thermal annealed bimagnetic core/shell nanoparticles

G. C. Lavorato*, E. Lima Jr., H. E. Troiani, R. D. Zysler and E. L. Winkler

Centro Atómico Bariloche, CNEA-CONICET, 8400 S.C. de Bariloche, Río Negro, Argentina

Abstract

In this study we demonstrate that the effective coupling of the magnetic phases in core/shell nanoparticles can be promoted by an appropriate thermal annealing. In this way, the magnetization thermal stability of the hard ferrimagnetic $CoFe_2O_4$ oxide can be increased up to room temperature when coupled to a CoO antiferromagnetic core in an inverse core/shell structure. In addition, the results show that, being encapsulated in a ~2 nm thick $CoFe_2O_4$ shell, the CoO core is successfully protected against oxidation which is crucial for the effectiveness of the magnetic coupling at the interface.

Keywords: Nanostructured materials, Chemical synthesis, Core-shell nanoparticles, Magnetization, Magnetic measurements, TEM.

1. Introduction

Bimagnetic core/shell nanoparticles (NPs) have acquired increasing interest due to the possibility of combining different materials and fabricating nanostructures with improved properties[1,2]. The tuning of the magnetic properties through the interface coupling of distinct magnetic materials has been widely studied, mainly in thin films[3]. However, chemical advances in the fabrication of NPs that involve thermal decomposition methods of

* Author to whom correspondence should be addressed. Tel.: +54 2944 445158. Electronic mail: lavorato@cab.cnea.gov.ar

organometallic compounds[4,5] have allowed greater control of the synthesis and the possibility of designing new bimagnetic NPs suitable for the development of permanent magnets[6], data storage applications[7], spin-valve sensors[8] and biomedical uses[9–11]. Since nanostructured systems are very sensitive to surface and interface phenomena and the magnetic coupling mechanism at the interface is not fully understood[12,13], several experimental works have been focused on the relationship between the crystalline structure, the morphology and the physical properties[5,9,14,15]. In many cases, core/shell NPs have been fabricated by a controlled oxidation of single-phase NPs [16–18] but seed-mediated multi-steps methods have also been used[19,20] leading to greater versatility in the combination of different materials. Some experimental studies on materials involving magnetic phases with different crystalline structures and morphologies have been performed on core/shell[17,21], singly inverted core/shell[16], doubly inverted core/shell[22], cubic core/shell [15] or self-assembled [23] particles. The comprehension of the mechanisms that govern the magnetic behavior of these nanostructures is crucial for the development of engineered materials for innovative applications. Inverted core/shell bimagnetic systems are particularly interesting since they permit a greater control of the structural properties of its AFM core (and thus of the overall magnetic properties) that, in general, is not easily attained in conventional structures[24,25]. In particular, inverted core/shell $CoO/CoFe_2O_4$ particles formed by two highly anisotropic magnetic materials (antiferromagnetic –AFM- CoO and ferrimagnetic –FiM- $CoFe_2O_4$) have been reported as good candidates for increasing the magnetic hardness[19,26]. Since the origin of such coercivity increase is associated with the exchange interaction at the interface[26,27], the effectiveness of the magnetic coupling should be strongly related to the crystalline structure of the material and therefore to the synthesis process.

In this work we have fabricated bimagnetic $CoO/CoFe_2O_4$ nanoparticles by a seed-mediated synthesis method with the aim of investigating the influence of thermal annealing on the interface magnetic coupling that rules the magnetic properties of the system. We show how the magnetic behavior is strongly influenced by the chemical composition and crystalline structure of the system.

2. Experimental

$CoO/CoFe_2O_4$ core/shell nanoparticles were synthesized by means of the high-temperature decomposition of metal acetylacetonates assisted by oleic acid and oleylamine as surfactants. The procedure consists on the mixture of 4 mmol of $Co(acac)_2$, 8 mmol of oleic acid, 8 mmol of oleylamine, 0.02 mmol of 1-2 octanediol and 116 mmol of 1-octadecene. Subsequently, the mixture was magnetically stirred and heated up to 200 °C for 10 minutes, then, it was heated up again to the reflux temperature (315 °C) with a controlled heating rate of 30 $°C \cdot min^{-1}$ and kept at that temperature for 120 minutes. Then, the mixture was cooled down to room temperature and a small portion of the obtained NPs was extracted for further analyses (sample *C*). In order to obtain core/shell NPs (sample *CF*), 0.8 mmol of $Co(acac)_2$ and 1.6 mmol of $Fe(acac)_3$ were added to the mixture according to the molar composition of the cobalt ferrite. In the same step, 0.02 mmol of 1-2 octanediol, 4 mmol of oleylamine, 4 mmol of oleic acid and 31 mmol of 1-octadecene were added and the preparation was heated up to 315 °C for another 120 min. In this second stage the heating rate was fixed at 30 $°C \cdot min^{-1}$ to promote the heterogeneous nucleation of the spinel phase on the seeds.

Afterwards, the NPs were precipitated by centrifugation (14000 rpm/ 30 min) and washed several times with a mixture of ethanol and toluene 8:1. With the objective of evaluating the effects of the thermal annealing on the magnetic properties of the core/shell NPs, both *C* and *CF* samples were heated up to 300 °C with a heating rate of 2.5 $°C \cdot min^{-1}$ and kept at that temperature for 2 hours in air atmosphere (samples *C-R* and *CF-R,* respectively). The

obtained powder was then mixed with an epoxy resin to prevent the mechanical movement of the nanoparticles during the magnetic characterization.

The crystalline structure was characterized by X-ray powder diffraction (XRD), using a PANalytical Empyrean diffractometer (CuKα radiation). The core/shell morphology and particle size distribution were assessed by means of a Philips CM200 UT transmission electron microscope (TEM) operating at 200 kV. The crystallinity and morphology of the samples were evaluated by high-resolution and dark-field TEM images. The magnetic behavior was analyzed using a superconducting quantum interference device (SQUID, Quantum Design) magnetometer in the temperature range of 5 K to 330 K and a LakeShore VSM with a ±10 kOe maximum applied field in the temperature range 250-320 K. Magnetization versus temperature experiments were performed following the ZFC (zero field cooling) and FC (field cooling) procedures for both as-produced and annealed samples at applied fields of 100 Oe and 5 kOe. TRM (thermoremanent magnetization) measurements were performed by cooling the sample from 330 to 5 K under 100 Oe applied field and subsequently measuring the magnetization during heating at zero applied field.

3. Results

Fig. 1a shows the XRD patterns of the as-synthesized and thermal annealed CoO NPs, *C* and *C-R* samples respectively. For comparison, the diffraction peaks of bulk Fm-3m CoO and Fd-3m Co_3O_4 phases were included. In the as-synthesized sample only the diffraction peaks of the CoO phase could be identified which are broad and barely resolved. After the thermal treatment, although the CoO diffraction pattern is detected, the predominant phase is Co_3O_4 indicating that Co^{2+} was oxidized during the annealing. **Fig. 1b** shows the XRD patterns of the as-synthesized (*CF*) and annealed (*CF-R*) core/shell CoO/$CoFe_2O_4$ nanoparticles. The XRD peaks can be indexed by the bulk Fm-3m CoO and Fd-3m $CoFe_2O_4$ reflections. It is noteworthy from **Fig. 1b** that, after the annealing, the CoO diffraction peaks are notably

better defined, narrower and their intensity grows relatively to the $CoFe_2O_4$ peaks, suggesting a higher degree of crystalline order for the CoO structure. Regarding the crystalline structure, it is observed that the diffraction peaks' positions of both phases for sample *CF* match well with the expected values of its bulk counterparts. However, after the thermal treatment, only CoO peaks reproduce the bulk positions, while $CoFe_2O_4$ peaks are broader and shifted approximately $\Delta(2\theta)\sim 0.2^{o}$ from the expected bulk values. As a consequence, for example, the $CoFe_2O_4$ interplanar distance d_{311} calculated from the diffraction peak shift decreases from 2.534 Å to 2.524 Å after the annealing.

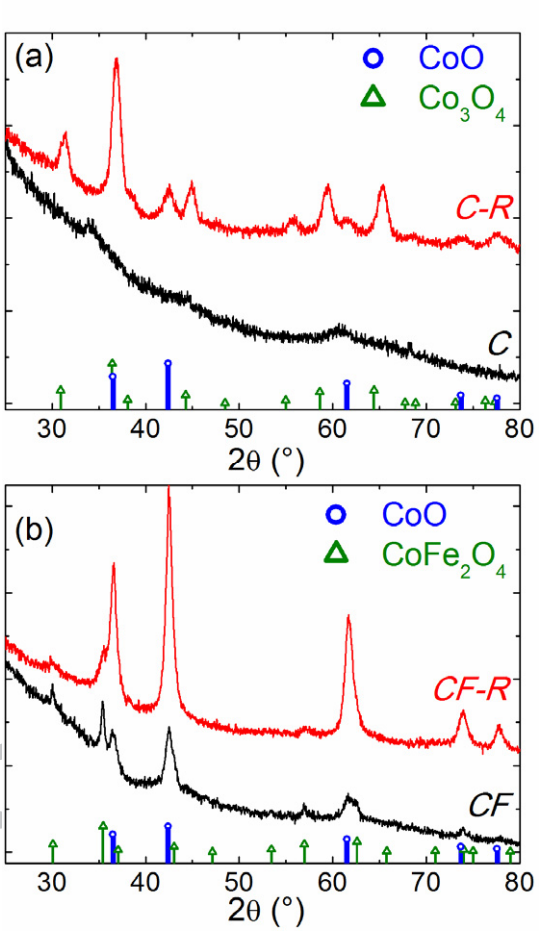

Fig. 1. X-Ray diffraction patterns of (a) as-synthesized cores (C) and annealed cores (C-R) and (b) as-synthesized core/shell (*CF*) and annealed core/shell (*CF-R*) nanoparticles. Thick lines indicate the reflections for bulk CoO, $CoFe_2O_4$ and Co_3O_4.

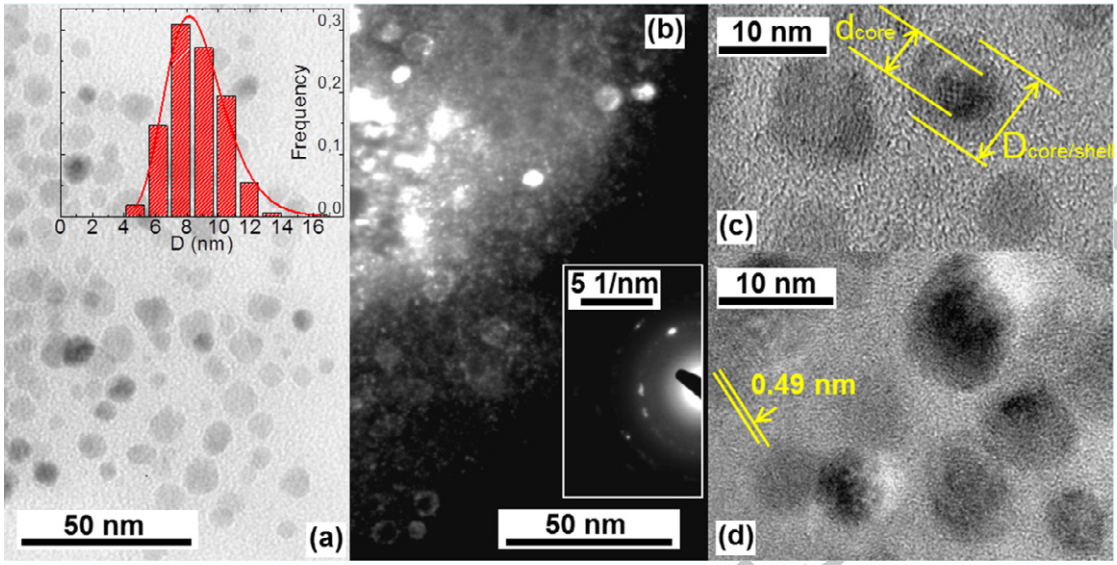

Fig. 2. TEM micrographs of annealed CoO/$CoFe_2O_4$ core/shell nanoparticles (sample *CF-R*): (a) bright field image and size distribution, (b) dark-field image obtained from the contrast generated by 111 planes of $CoFe_2O_4$ and (inset) electron diffraction pattern and (c-d) high resolution images that reveal the core/shell structure.

TEM micrographs corresponding to annealed core/shell NPs are shown in **Fig. 2**. The particle size dispersion was evaluated by measuring hundreds of particles and it is reported in **Fig. 2a**. The obtained histogram was fitted with a lognormal function and a mean size of 8.7±1.9 nm was calculated. To analyze the core/shell structure, high resolution and dark field TEM images were measured and representative images are displayed in **Fig. 2b-d**. The $CoFe_2O_4$ shell morphology was confirmed by dark field images reconstructed by positioning a small objective aperture on the 111 $CoFe_2O_4$ diffraction ring. A shell thickness of ~2 nm was estimated from numerous dark field and HRTEM images. Moreover, the images reveal that the particles are separated by residual amorphous carbon from the synthesis that would prevent the coalescence of NPs. Finally, it should be noticed that the core/shell nanoparticle size is larger than ~7 nm NPs obtained by the same method but employing a different solvent with a lower reflux temperature[19].

Fig. 3 presents the magnetization measurements for *CF* and *CF-R* samples. The temperature dependence of the magnetization for the *CF* as-prepared sample, presented in **Fig. 3a**, shows the typical behavior of an assembly of weakly interacting magnetic nanoparticles, where the magnetic moments block progressively when the temperature diminishes according to their energy barrier distribution. The ZFC magnetization curve presents a maximum which is related to the mean blocking temperature, $<T_B>$, and the FC magnetization increases when the temperature is decreased, as expected for non- or weakly-interacting particles. Moreover, a slight magnetization increase is observed at low temperature either for ZFC and FC curves; this feature is more evident when the measurement is performed with a higher applied field, as seen in **Fig. 3c**. The energy barrier distribution, showed in the inset of **Fig. 3e**, was obtained from the remanence curve according to: $f(T_B) \sim (1/T)[dM_{TRM}/dT]$, where $<T_B> \sim 170$ K was determined as the median value of the distribution[28] for the as-synthesized core/shell sample.

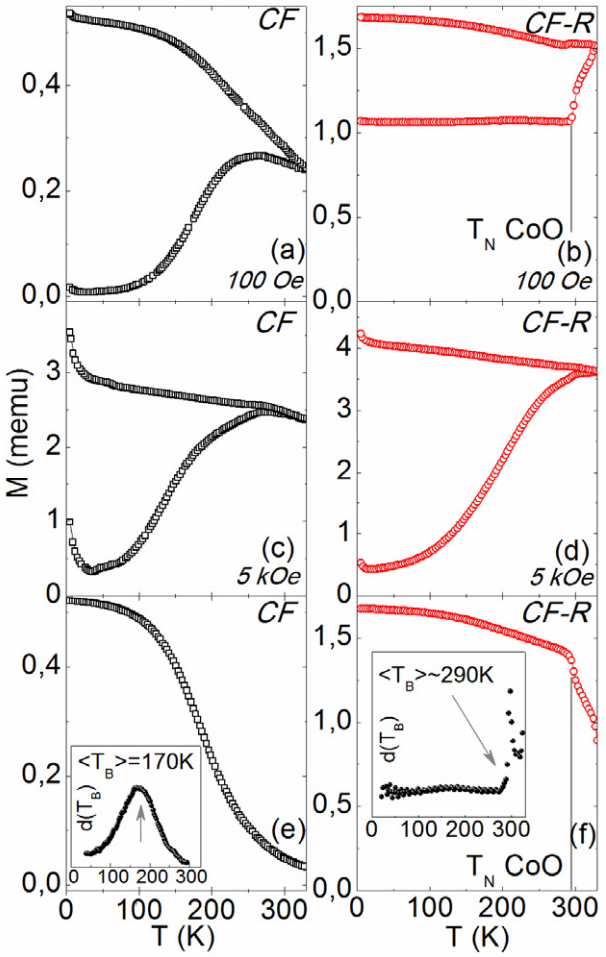

Fig. 3. Temperature dependence of the magnetization for as-synthesized (*CF*) and annealed (*CF-R*) CoO/$CoFe_2O_4$ core/shell nanoparticles: (a-b) ZFC-FC at 100 Oe, (b-c) ZFC-FC at 5 kOe, (e-f) TRM at 100 Oe and (insets) distribution of blocking temperatures obtained from TRM measurements.

On the other hand, the magnetization of the annealed sample *CF-R*, presented in **Fig. 3b**, exhibits a different behavior. When the temperature increases the ZFC magnetization shows an abrupt rise around 290 K that can be related to the Néel temperature of CoO (T_{N_bulk}~293 K)[29]. The temperature dependence of the FC magnetization curve presents a small anomaly at T_N and when the temperature diminishes it shows a nearly flat behavior suggesting that the system is strongly interacting below T_N. The remanent magnetization curve is displayed in

Fig. 3f: when the temperature is raised the magnetization decreases slowly up to 290 K, where a sudden drop is observed coincidently with the T_N of CoO. The temperature derivative of TRM (inset of **Fig. 3f**) evidences a sharp peak at T~290 K which implies that the blocking temperature of the annealed core/shell nanoparticles has been shifted to T_N. These results are consistent with the presence of intra-particle interactions that improve the thermal stability of the magnetization at temperatures below T_N, *i.e.* when the magnetic coupling at the AFM/FiM interface is active. In addition, a small maximum at a lower temperature T~174K can be noticed, which could be associated to a small fraction of the $CoFe_2O_4$ phase that is not effectively coupled to the AFM CoO.

In order to gain better insight of the magnetic coupling, hysteresis cycles were measured at temperatures around T_N for *CF* and *CF-R* samples. The field dependence of the magnetization for the as-synthesized *CF* sample presents constricted loops at low fields that show essentially the same shape above and below T_N (**Fig. 4b**). In this case, the coercive field changes from 0.3 kOe to 0.6 kOe when the temperature decreases from 310 K to 250 K. On the contrary, the annealed sample presents a typical smooth hysteresis curve at 250 K with a coercive field (H_C~2.5 kOe) more than four times larger than the value measured for the as-synthesized sample. However, above T_N the M vs H curve of *CF-R* also presents a constricted loop shape (**Fig. 4a**). These features are reflected in the temperature variation of coercivity presented in **Fig. 5**. The coercivity of *CF-R* shows a step at the CoO Néel temperature but no significant changes are observed for *CF*.

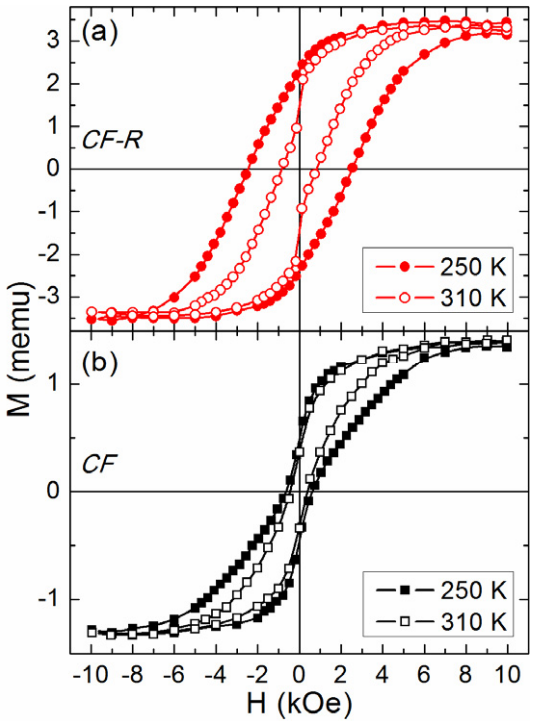

Fig. 4. Hysteresis loops of (a) annealed $CoO/CoFe_2O_4$ nanoparticles (sample *CF-R*) and (b) as-synthesized $CoO/CoFe_2O_4$ nanoparticles (sample *CF*) recorded at 250 K (full symbols) and 310 K (empty symbols).

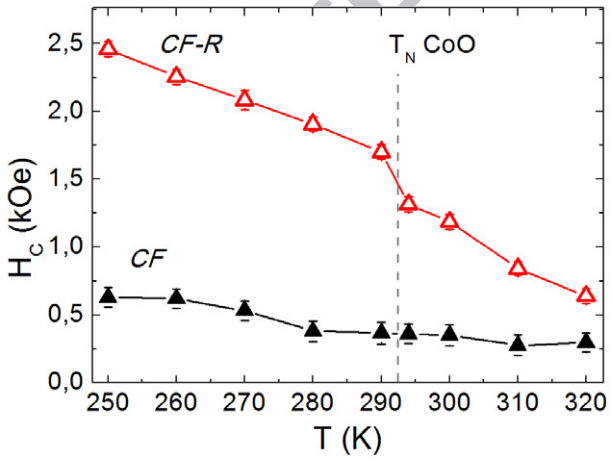

Fig. 5. Temperature dependence of the coercive field between 250 K and 320 K for annealed (open symbols) and as-produced (full symbols) $CoO/CoFe_2O_4$ bimagnetic nanoparticles.

4. Discussion

The CoO, due to its high magnetocrystalline anisotropy, is a good candidate to increase the magnetic hardness of a ferrimagnetic nanostructure by the interface exchange-coupling. However, the crystallinity and chemical stability of the AFM phase are essential and determine the effectiveness of the magnetic coupling at the interface. According to the structural and magnetic characterization, our findings suggest that the core of the as-produced CoO/$CoFe_2O_4$ sample is poorly crystalline and a proper thermal treatment is required to improve its crystalline order. In fact, as evidenced by the XRD patterns in **Fig. 1b**, the CoO diffractions peaks are much better defined after the annealing. Moreover, the presence of the crystalline CoO core would promote a slight distortion in the spinel structure, in agreement with the observed shifts of the $CoFe_2O_4$ diffraction peaks from its bulk positions. The induced distortions in the spinel lattice would be introducing strain into the crystalline structure leading to the peak broadening displayed by $CoFe_2O_4$ in *CF-R*. In relation to the CoO chemical stability, it is noteworthy that the encapsulation of CoO in the $CoFe_2O_4$ shell prevents the oxidation of the core material. In fact, while sample *CF-R* shows an increased CoO crystallinity, as a consequence of the same thermal annealing *C-R* reveals a partial oxidation to the Co_3O_4 phase, which is paramagnetic at room temperature. Therefore, an inverted core/shell structure is a successful option to protect the antiferromagnetic phase against oxidation, to achieve a high crystallinity and to improve the effectiveness of the interface interactions.

The structural characterization can clarify some observed magnetic features for the as-produced sample. The low temperature magnetization rise observed in **Fig. 3** for the as-synthesized sample could be ascribed to the contribution of paramagnetic Co ions due to the structural disorder of the CoO phase. On the contrary, the annealed sample exhibits a strongly coupled two-phase behavior and a much smaller low temperature magnetization rise. While a

mean blocking temperature of $<T_B>_{CF}$ ~170K was obtained for as-synthesized sample, the strong magnetic coupling in the annealed sample enhances its energy barrier and shifts $<T_B>_{CF-R}$ up to values close to room temperature. The increased thermal stability is further evidenced by comparing our findings on a ~2 nm thick $CoFe_2O_4$ shell with blocking temperatures reported in literature for single phase ~8 nm NPs having the same $CoFe_2O_4$ volume. Superparamagnetic relaxation of cobalt ferrite NPs has been widely studied and, for example, $<T_B>$ varies from 150 K to 315 K for particles between 5.7 nm and 12.7 nm[30–32]; 7.5 nm single-phase $CoFe_2O_4$ NPs fabricated by a thermal decomposition method present a $<T_B>$ of ~200 K[33], remarkably lower than the mean blocking temperature of $CoO/CoFe_2O_4$ NPs in this study that has been shifted up to room temperature.

Regarding the field dependence of the magnetization, both *CF* and *CF-R* NPs present at room temperature a shrinking of the hysteresis cycle at low fields. This feature is usually observed in inhomogeneous materials with two weakly coupled soft-hard magnetic phases[9,34]. Since the loop shrinking, in our samples, is observed above T_N, we ascribe the two phase behavior to inner and surface contributions of $CoFe_2O_4$ magnetization. Due to the strong magnetocrystalline contribution, the inner part of the cobalt ferrite phase should have a magnetic anisotropy higher than the one of the outer part, which may be reduced because of surface disorder and the presence of the organic coating. Similar features were observed in single phase nanoparticles and thin films with different surface and bulk magnetic anisotropy contributions[35–37].

The small H_C and the smooth temperature dependence around T_N displayed by the as-produced sample should be related to the absence of AFM/FiM exchange-interaction, possibly originated by the lack of AFM order of CoO or by the surface disorder promoted by its reduced size. After the annealing, the AFM/FiM coupling at the interface is more effective and, as a consequence, the effective magnetic anisotropy of the $CoFe_2O_4$ is increased below

T_N due to the additional exchange anisotropy contribution[27]. Such hardening of the exchange-coupled material is noticeable because the CoO anisotropy constant K_{CoO}~$4 \cdot 10^7$ erg·cm^{-3} [38] is an order of magnitude higher than $K_{CoFe2O4}$~$4 \cdot 10^6$ erg·cm^{-3} [39]. The hardening of the exchange-coupled material is also clearly manifested by the step-increase of the coercive field close to T_N. In this sense, the essential characteristic of the annealed sample is a hardening of the magnetic properties and an increased stability of the magnetization up to the CoO Néel temperature.

5. Conclusion

We have fabricated inverted core/shell nanoparticles and studied the effect of a thermal annealing on its crystalline and magnetic properties. We have shown that, in this particular system, the annealing is essential to improve the crystalline structure of the CoO phase and, as a consequence, to achieve an effective AFM/FiM interface coupling and to enhance the magnetic thermal stability. In fact, the blocking temperature of the FiM shell can be shifted from ~170 K to nearly room temperature by controlling the crystallinity of the AFM core. We have also demonstrated that the FiM $CoFe_2O_4$ shell protects the CoO hard AFM phase against oxidation in the inverted core/shell structure. Finally, we remark that CoO/$CoFe_2O_4$ bimagnetic nanoparticles show magnetic hardening and thermal stability enhancement as compared to bigger single phase nanoparticles, opening new possibilities to design novel materials for permanent magnets and magnetic data storage.

Acknowledgments

The authors thank ANPCyT Argentina through Grant PICT 2012-0492, CONICET Argentina through Grant PIP 112-20110100519 and UNCuyo Argentina through Grants 06-C404 and C011.

References

[1] A.-H. Lu, E.L. Salabas, F. Schüth, Magnetic nanoparticles: synthesis, protection, functionalization, and application., Angew. Chem. Int. Ed. Engl. 46 (2007) 1222–44. doi:10.1002/anie.200602866.

[2] A. López-Ortega, M. Estrader, G. Salazar-Alvarez, A.G. Roca, J. Nogués, Applications of exchange coupled bi-magnetic hard/soft and soft/hard magnetic core/shell nanoparticles, Phys. Rep. (2014). doi:10.1016/j.physrep.2014.09.007.

[3] J. Nogués, I.K. Schuller, Exchange bias, J. Magn. Magn. Mater. 192 (1999) 203–232. doi:10.1016/S0304-8853(98)00266-2.

[4] S. Sun, H. Zeng, Size-controlled synthesis of magnetite nanoparticles, J. Am. Chem. Soc. (2002) 8204–8205. http://pubs.acs.org/doi/abs/10.1021/ja026501x.

[5] T. Hyeon, Chemical synthesis of magnetic nanoparticles, Chem. Commun. (2003) 927–934. doi:10.1039/b207789b.

[6] H. Zeng, J. Li, J. Liu, Z. Wang, S. Sun, Exchange-coupled nanocomposite magnets by nanoparticle self-assembly, Nature. 420 (2002) 395–398. doi:10.1038/nature01233.1.

[7] V. Skumryev, S. Stoyanov, Y. Zhang, Beating the superparamagnetic limit with exchange bias, Nature. 423 (2003) 19–22. doi:10.1038/nature01750.1.

[8] J. Kools, Exchange-biased spin-valves for magnetic storage, Magn. IEEE Trans. 32 (1996) 3165–3184. http://ieeexplore.ieee.org/xpls/abs_all.jsp?arnumber=508381.

[9] Q. Song, Z.J. Zhang, Controlled synthesis and magnetic properties of bimagnetic spinel ferrite $CoFe_2O_4$ and $MnFe_2O_4$ nanocrystals with core-shell architecture., J. Am. Chem. Soc. 134 (2012) 10182–90. doi:10.1021/ja302856z.

[10] J. Gao, H. Gu, B. Xu, Multifunctional magnetic nanoparticles: design, synthesis, and biomedical applications., Acc. Chem. Res. 42 (2009) 1097–107. doi:10.1021/ar9000026.

[11] J.H. Lee, J.T. Jang, J.S. Choi, S.H. Moon, S.H. Noh, J.W. Kim, et al., Exchange-coupled magnetic nanoparticles for efficient heat induction., Nat. Nanotechnol. 6 (2011) 418–22. doi:10.1038/nnano.2011.95.

[12] M. Estrader, A. López-Ortega, S. Estradé, I. V Golosovsky, G. Salazar-Alvarez, M. Vasilakaki, et al., Robust antiferromagnetic coupling in hard-soft bi-magnetic core/shell nanoparticles., Nat. Commun. 4 (2013) 2960. doi:10.1038/ncomms3960.

[13] J. Nogués, J. Sort, V. Langlais, V. Skumryev, S. Suriñach, J.S. Muñoz, et al., Exchange bias in nanostructures, Phys. Rep. 422 (2005) 65–117. doi:10.1016/j.physrep.2005.08.004.

[14] H. Tüysüz, E.L. Salabaş, E. Bill, H. Bongard, B. Spliethoff, C.W. Lehmann, et al., Synthesis of Hard Magnetic Ordered Mesoporous Co 3 O 4 /CoFe 2 O 4 Nanocomposites, Chem. Mater. 24 (2012) 2493–2500. doi:10.1021/cm3005166.

[15] S.-H. Noh, W. Na, J.-T. Jang, J.-H. Lee, E.J. Lee, S.H. Moon, et al., Nanoscale magnetism control via surface and exchange anisotropy for optimized ferrimagnetic hysteresis., Nano Lett. 12 (2012) 3716–21. doi:10.1021/nl301499u.

[16] D. Kavich, J. Dickerson, S. Mahajan, S. Hasan, J.-H. Park, Exchange bias of singly inverted FeO/Fe_3O_4 core-shell nanocrystals, Phys. Rev. B. 78 (2008) 174414. doi:10.1103/PhysRevB.78.174414.

[17] Q. Ong, A. Wei, X.-M. Lin, Exchange bias in Fe/Fe3O4 core-shell magnetic nanoparticles mediated by frozen interfacial spins, Phys. Rev. B. 80 (2009) 134418. doi:10.1103/PhysRevB.80.134418.

[18] A. López-Ortega, D. Tobia, E. Winkler, I. V Golosovsky, G. Salazar-Alvarez, S. Estradé, et al., Size-dependent passivation shell and magnetic properties in antiferromagnetic/ferrimagnetic core/shell MnO nanoparticles., J. Am. Chem. Soc. 132 (2010) 9398–407. doi:10.1021/ja1021798.

[19] E. Lima, E.L. Winkler, D. Tobia, H.E. Troiani, R.D. Zysler, E. Agostinelli, et al., Bimagnetic CoO Core/$CoFe_2O_4$ Shell Nanoparticles: Synthesis and Magnetic Properties, Chem. Mater. 24 (2012) 512–516. doi:10.1021/cm2028959.

[20] W. Baaziz, B.P. Pichon, C. Lefevre, C. Ulhaq-Bouillet, J.-M. Greneche, M. Toumi, et al., High Exchange Bias in $Fe_{3-\delta}O_4$@CoO Core Shell Nanoparticles Synthesized by a One-Pot Seed-Mediated Growth Method, J. Phys. Chem. C. 117 (2013) 11436–11443. doi:10.1021/jp402823h.

[21] S. Inderhees, J. Borchers, K. Green, M. Kim, K. Sun, G. Strycker, et al., Manipulating the Magnetic Structure of Co Core/CoO Shell Nanoparticles: Implications for Controlling the Exchange Bias, Phys. Rev. Lett. 101 (2008) 117202. doi:10.1103/PhysRevLett.101.117202.

[22] A. Berkowitz, G. Rodriguez, J. Hong, K. An, T. Hyeon, N. Agarwal, et al., Antiferromagnetic MnO nanoparticles with ferrimagnetic Mn_3O_4 shells: Doubly inverted core-shell system, Phys. Rev. B. 77 (2008) 024403. doi:10.1103/PhysRevB.77.024403.

[23] J. Chen, X. Ye, S.J. Oh, J.M. Kikkawa, C.R. Kagan, C.B. Murray, Bistable magnetoresistance switching in exchange-coupled $CoFe_2O_4$ - Fe_3O_4 binary nanocrystal superlattices by self-assembly and thermal annealing., ACS Nano. 7 (2013) 1478–86. doi:10.1021/nn3052617.

[24] J. Nogués, V. Skumryev, J. Sort, S. Stoyanov, D. Givord, Shell-Driven Magnetic Stability in Core-Shell Nanoparticles, Phys. Rev. Lett. 97 (2006) 157203. doi:10.1103/PhysRevLett.97.157203.

[25] G. Margaris, K.N. Trohidou, J. Nogués, Mesoscopic model for the simulation of large arrays of bi-magnetic core/shell nanoparticles., Adv. Mater. 24 (2012) 4331–6. doi:10.1002/adma.201200615.

[26] G.C. Lavorato, E. Lima Jr, D. Tobia, D. Fiorani, H.E. Troiani, R.D. Zysler, et al., Size effects in bimagnetic CoO/$CoFe_2O_4$ core/shell nanoparticles., Nanotechnology. 25 (2014) 355704. doi:10.1088/0957-4484/25/35/355704.

[27] E.L. Winkler, E. Lima, D. Tobia, M.E. Saleta, H.E. Troiani, E. Agostinelli, et al., Origin of magnetic anisotropy in ZnO/$CoFe_2O_4$ and CoO/$CoFe_2O_4$ core/shell nanoparticle systems, Appl. Phys. Lett. 101 (2012) 252405. doi:10.1063/1.4771993.

[28] J.L. Dormann, D. Fiorani, E. Tronc, Magnetic relaxation in fine-particle systems. Advanced in Chemical Physics vol XCVIII, Wiley, New York, 1997.

[29] J. Goodenough, Metallic oxides, Prog. Solid State Chem. 5 (1971) 145–399. doi:10.1016/0079-6786(71)90018-5.

[30] C.R. Vestal, Q. Song, Z.J. Zhang, Effects of Interparticle Interactions upon the Magnetic Properties of CoFe 2 O 4 and MnFe 2 O 4 Nanocrystals, J. Phys. Chem. B. 108 (2004) 18222–18227. doi:10.1021/jp0464526.

[31] D. Peddis, F. Orrù, A. Ardu, C. Cannas, A. Musinu, G. Piccaluga, Interparticle Interactions and Magnetic Anisotropy in Cobalt Ferrite Nanoparticles: Influence of Molecular Coating, Chem. Mater. 24 (2012) 1062–1071. doi:10.1021/cm203280y.

[32] T.E. Torres, A.G. Roca, M.P. Morales, A. Ibarra, C. Marquina, M.R. Ibarra, et al., Magnetic properties and energy absorption of $CoFe_2O_4$ nanoparticles for magnetic hyperthermia, J. Phys. Conf. Ser. 200 (2010) 072101. doi:10.1088/1742-6596/200/7/072101.

[33] B.N. Pianciola, E. Lima, H.E. Troiani, L.C.C.M. Nagamine, R. Cohen, R.D. Zysler, Size and surface effects in the magnetic order of $CoFe_2O_4$ nanoparticles, J. Magn. Magn. Mater. 377 (2015) 44–51. doi:10.1016/j.jmmm.2014.10.054.

[34] E. Kneller, R. Hawig, The exchange-spring magnet: a new material principle for permanent magnets, Magn. IEEE Trans. 27 (1991) 3588–3600. http://ieeexplore.ieee.org/xpls/abs_all.jsp?arnumber=102931.

[35] L. Horng, G. Chern, M.. Chen, P.. Kang, D.. Lee, Magnetic anisotropic properties in Fe_3O_4 and $CoFe_2O_4$ ferrite epitaxy thin films, J. Magn. Magn. Mater. 270 (2004) 389–396. doi:10.1016/j.jmmm.2003.09.005.

[36] F. Rigato, J. Geshev, V. Skumryev, J. Fontcuberta, The magnetization of epitaxial nanometric CoFe2O4 (001) layers, J. Appl. Phys. 106 (2009) 113924. doi:10.1063/1.3267873.

[37] K. Nadeem, M. Shahid, M. Mumtaz, Competing crystallite size and zinc concentration in silica coated cobalt ferrite nanoparticles, Prog. Nat. Sci. Mater. Int. 24 (2014) 199–204. doi:10.1016/j.pnsc.2014.05.011.

[38] J. Tracy, D. Weiss, D. Dinega, M. Bawendi, Exchange biasing and magnetic properties of partially and fully oxidized colloidal cobalt nanoparticles, Phys. Rev. B. 72 (2005) 064404. doi:10.1103/PhysRevB.72.064404.

[39] R. O'Handley, Modern Magnetic Materials: Principles and Applications, John Wiley & Sons, New Jersey, 1999.

Highlights

AFM/FiM CoO/$CoFe_2O_4$ nanoparticles were obtained by a seed-mediated decomposition method

The exchange coupling between the magnetic phases could be promoted by a thermal annealing

The FiM shell prevents the AFM core from oxidizing during a thermal annealing

The thermal stability of the FiM shell was increased by controlling the crystallinity of the AFM core